Self-Assembled Nanocarriers of Synthetic and Natural Plasmalogens for Potential Nanomedicine Development

Yu Wu, Borislav Angelov, Yuru Deng, Takehiko Fujino, Md Shamim Hossain, Thomas Bizien, Angelina Angelova

ADVANCED THERAPEUTICS
www.advtherap.com

Self-Assembled Nanocarriers of Synthetic and Natural Plasmalogens for Potential Nanomedicine Development

*Yu Wu, Borislav Angelov, Yuru Deng, Takehiko Fujino, Md Shamim Hossain, Thomas Bizien, and Angelina Angelova**

Plasmalogens are bioactive glycerophospholipids with a vinyl ether bond at the *sn-1* position of the glycerol backbone, which imparts free-radical scavenging properties. Amelioration of the plasmalogen levels, which decline with aging, is required for novel metabolic therapies for Parkinson's disease (PD), Alzheimer's disease (AD), and dementia. This work designed, prepared, and in vitro characterized plasmalogen-loaded lipid nanoparticles with neuroprotective potential for neuronanomedicine. Liquid crystalline nanoparticles formed by natural scallop-derived plasmalogens are in vitro evaluated with respect to synthetic docosapentaenoyl (DPA) plasmenyl (vinyl ether) glycerophospholipids, formulated with the helper lipid monoolein (MO). The structural organization of the lipid nanoparticles is characterized by synchrotron small-angle X-ray scattering (SAXS). The employed self-assembly technique yielded plasmalogen-based nanoassemblies of hexosome, cubosome, vesicular, or intermediate topology types. The internalization of fluorescently-labeled nanoparticles in differentiated human neuroblastoma SH-SY5Y cells is followed by flow cytometry. Under the investigated conditions, the scallop-derived plasmalogen nanocarriers significantly influenced the measured mitochondrial membrane potential compared to those involving synthetic plasmalogens with DPA chains. Levels of protein biomarkers, such as brain-derived neurotrophic factor (BDNF), can be regulated depending on the nanocarrier type. The results identified cubosome, hexosome, and vesicular types of plasmalogen nanocarriers presenting antioxidant properties and preserving neuronal cell integrity and viability.

1. Introduction

Lipid nanoassemblies are intensively used as excipients of therapeutic compounds thanks to their inherent biocompatibility and biodegradability, low immunogenicity, negligible toxicity, and capability to entrap guest molecules in their bilayer structure, which mimics the cellular membranes.[1–5] Among these, lipid nanoparticles (NPs) made of lyotropic amphiphilic mixtures, such as monoglyceride or phospholipid/cholesterol assemblies, have been broadly investigated for the delivery of mRNA vaccines, siRNA and CRISPR therapeutics, plasmid DNA, antibodies, peptides, and proteins.[6–12] In many cases, the phospholipid-based nanocarriers have been of liposome or solid lipid nanoparticle types.[6,13–15] In recent years, lyotropic nonlamellar lipids, which form liquid crystalline nanocarriers with inner 3D membrane architectures, have attracted increasing attention.[16–19] Self-assembly and dispersion of nonlamellar lipids in an aqueous medium can either yield cubosome or spongosome nanoparticles (derived from cubic and sponge mesophases) or hexosomes (particles with inverted hexagonal packing of lipid cylinders).[20–24]

Y. Wu, A. Angelova
Université Paris-Saclay, CNRS
Institut Galien Paris-Saclay
Orsay 91400, France
E-mail: angelina.angelova@universite-paris-saclay.fr
B. Angelov
Department of Structural Dynamics
Extreme Light Infrastructure ERIC
Dolni Brezany 25241, Czech Republic

Y. Deng
Wenzhou Institute
University of Chinese Academy of Sciences
No.1 Jinlian Road, Longwan District, Wenzhou, Zhejiang 325001, China
T. Fujino, M. S. Hossain
Institute of Rheological Functions of Food
2241-1 Kubara, Hisayama-cho, Kasuya-gun, Fukuoka 811-2501, Japan
T. Fujino
BOOCS Clinic
6F 6–18 Tenyamachi, Hakata-ku, Fukuoka 812-0025, Japan
T. Bizien
Synchrotron SOLEIL
l'Orme des Merisiers, Saint-Aubin 91192, France

The ORCID identification number(s) for the author(s) of this article can be found under https://doi.org/10.1002/adtp.202400093

DOI: 10.1002/adtp.202400093

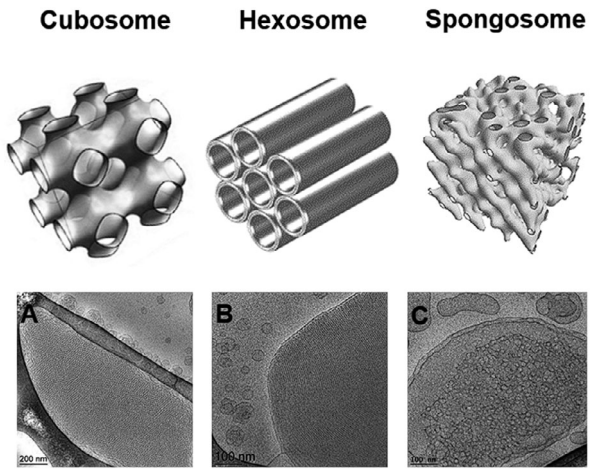

Figure 1. (Top) Schematic presentation of liquid crystalline nanocarriers with inner cubic (cubosome), inverted hexagonal (hexosome), or bicontinuous sponge membrane (spongosome) structural organization arising from the lyotropic lipid polymorphism. (Bottom) Typical cryo-TEM images demonstrating the inner self-assembled organization of lipid bilayers or tubes in bicontinuous cubic A), inverted hexagonal B), and sponge-type C) structures.[32]

The nanoparticle topology (cubosome, hexosome, spongosome, or other types), as depicted in **Figure 1**, can have a crucial impact on the drug release properties and the resident time and interactions of the drug delivery carriers with biological barriers.[5,25–28] Compared to liposomes, nonlamellar nanocarriers display enhanced capacity for encapsulation of active molecules such as peptides, proteins, nucleic acids, or small molecule compounds.[29–31]

It should be emphasized that lipids are not only passive carriers of drugs but can exert important health-beneficial functions.[32–35] Among them, vinyl ether type glycerophospholipids (involving a vinyl-ether linked alkyl chain in the position *sn-1*), and called plasmalogens, have been shown to hamper the cellular apoptosis signaling pathways[36–38] and lipid oxidation,[39] impede the formation of neurotoxic β-amyloid aggregates,[40] promote neurogenesis and axonal guidance,[41,42] and exert neuroprotection against degenerative disorders.[43–45] Plasmalogens are implicated in the pathogenesis of several diseases provoked by brain phospholipid dysregulation,[46,47] oxidative stress,[48] neuroinflammation,[49,50] disturbed neurotransmitter homeostasis,[51] synaptic defects,[43] cognitive deficiency[52] as well as peroxisomal disorders.[40,53] Altered plasmalogen content in the neuronal cell membranes may contribute to neurodegeneration, and plasmalogen deficiency may be a causative factor for neurodegeneration in AD and dementia.[54] Reduced levels of plasmalogens have been indeed observed in AD and PD patients.[55] Important biological functions of plasmalogens include the improvement of learning and memory capacities of aged individuals[53] and protection from cardiometabolic and neuromuscular impairments.[36] In clinical studies, oral administration of scallop-derived plasmalogens has been established to considerably enhance the cognitive functions of AD patients.[42,54,56] It is desirable to ameliorate the plasmalogen levels in AD patients by endogenous delivery. However, the vinyl ether phospholipids with long PUFA chains are of low chemical stability and therefore require the development of delivery carriers enabling their therapeutic application in nanomedicine.

The present work aims at nanoformulation of purified scallop-derived plasmalogens by the lipid self-assembly method, exploiting lyotropic lipid polymorphism. An initial in vitro biological evaluation of the plasmalogen-loaded nanocarrier systems is performed in view of potential nanomedicine applications. The purpose is to find out the structural organization of stable nanoparticulate formulations and safe amphiphilic compositions suitable for nanomedicine development. The internalization kinetics of the lipid nanoparticles and the related mitochondrial membrane potential (MMP) changes were investigated by flow cytometry to compare the interaction of neuronally-derived cells with natural and synthetic plasmalogen-based nanoassemblies. Lipid nanoparticle-mediated regulation of neurotrophic proteins, e.g. brain-derived neurotrophic factor (BDNF), was of particular interest to this work.

2. Experimental section

2.1. Materials

The vinyl ether glycerophospholipids 1-O-1′-(Z)-hexadecenyl-2-(4Z,7Z,10Z,13Z,16Z-docosapentaenoyl)-sn-glycero-3-phosphocholine, C16:1p-22:5n6 PC (M.W. 791.58) and 1-O-1′-(Z)-hexadecenyl-2-(4Z,7Z,10Z,13Z,16Z-docosapentaenoyl)-sn-glycero-3-phosphoethanolamine, C16:1p-22:5n6 PE, (M.W. 749.54) were custom synthesized by Avanti Polar Lipids, Inc. (Alabama) together with 1,2-bis(4Z,7Z,10Z,13Z,16Z-docosapentaenoyl)-sn-glycero-3-phosphoinositol (ammonium salt), di-22:5n6 PI, (M.W. 958.56). These synthetic glycerophospholipids with DPA chains were received as lipid solutions in chloroform. They were abbreviated as DPA-pPC, DPA-pPE and DPA-PI in Table S1 (Supporting Information). The lipids were of high purity (>99%) and were characterized via TLC, MS, and NMR analyses by the provider. The fluorescent lipid 1,2-dioleoyl-sn-glycero-3-phosphoethanolamine-N-(lissamine rhodamine B sulfonyl) (ammonium salt) (18:1 Liss Rhod PE) was also purchased from Avanti Polar Lipids, Inc. (Alabama). Monoolein (MO, C18:1c9, MW 356.54, powder, ≥99%), retinoic acid (RA), vitamin E (VitE), curcumin (CU), coenzyme Q_{10} (Q_{10}), 2,6-di-tert-butyl-4-methylphenol (BHT), Pluronic F167, and D-α-tocopherol polyethylene glycol-1000 succinate (TPGS-PEG_{1000}) were purchased from Sigma–Aldrich. Other PEGylated lipids, serving as biocompatible dispersing and stabilizing agents, were received from NOF Corporation (Tokyo, Japan), namely poly(ethylene glycol)monooleate NHS derivative (MO-PEG_{2000}, Sunbright OE-020CS) and N-(methylpolyoxyethylene oxycarbonyl)-1,2-distearoyl-sn-glycero-3-phosphoethanolamine, sodium salt (Sunbright DSPE-PEG_{2000}). Water of MilliQ quality (Millipore Corp., Molsheim, France) was used for the preparation of a phosphate buffer solution (NaH_2PO_4/Na_2HPO_4, 1×10^{-2} M, pH 7, p.a. grade, Merck). The latter contained the antioxidant BHT, which ensured the oxidative stability of the aqueous formulations by suppressing the formation of lipid hydroperoxides. The phosphate/BHT buffer medium was purged by nitrogen gas (to eliminate the dissolved oxygen) and filtered through a 0.2 μm sterile filter (Millipore Corp.).

The investigated natural extract had a lipid composition of purified ether phospholipids from scallops as established by Fujino et al.[54] The process that can sustainably store plasmalogen for an extended time has been developed at the Institute of Rheological Function of Food *Co Ltd*. Purified scallop-derived plasmalogens were available for our work from Prof. Fujino's lab. They were organic-solvent extracted and purified by a multi-step procedure as previously reported.[54] The composition of the scallop-derived plasmalogen extract was a mixture of ethanolamine ether phospholipid (49.4%), choline ether phospholipid (24.9%), cholesterol (16.0%), and ceramide aminoethyl phosphonate (CAEP) (9.7%). This natural plasmalogen combination of 70% vinyl ether phospholipid content was referred to in the following as scPL70 (see Table S1, Supporting Information). A small amount of highly purified scallop-derived plasmalogen with 100% vinyl-ether phospholipid content (scPL100), constituted by a mixture of plasmenyl phosphoethanolamines and phosphocholines, was also available for the structural experiments. The received purified plasmalogens (scallop-derived natural extracts) were dissolved in chloroform for preparation of nanoformulations by the self-assembly method as described below (see "Lipid nanoparticle sample preparation").

For cell culture experiments, Dulbecco's modified Eagle's Medium (DMEM), streptomycin-penicillin, phosphate buffered saline (PBS), trypsin, ethylenediaminetetraacetic acid EDTA, and 3-(4,5-Dimethylthiazol-2-yl)-2,5-diphenyl tetrazolium bromide (MTT) were supplied by Sigma–Aldrich. Fetal bovine serum (FBS) was provided by Thermo Fischer Scientific (Illkirch, France).

2.2. Lipid Nanoparticle Sample Preparation

Lipid NPs were prepared by the method of hydration of a lyophilized thin lipid film followed by physical agitation in the excess aqueous phase.[10,32] The lipids (plasmalogens and MO), the lipophilic antioxidants (VitE, CU, or Q_{10}), and the PEGylated amphiphilic agents (TPGS-PEG_{1000}, MO-PEG_{2000}, DSPE-PEG_{2000}, or Pluronic F167) were weighed, dissolved in chloroform, and mixed at desired proportions. The solvent was evaporated under a stream of nitrogen gas to create a thin lipid film. The samples were lyophilized overnight under cooling to remove the excess solvent. This step was followed by the hydration of the thin film mixtures by an aqueous phase (1×10^{-2} M phosphate buffer NaH_2PO_4/Na_2HPO_4, pH 7, with added BHT). The buffer was purged and manipulated under a nitrogen gas atmosphere in order to prevent oxidation of the vinyl ether bonds of the plasmalogens.

For dispersion to NPs, the hydrated lipid mixtures were subjected to vortexing and agitation in an ice bath in repeating cycles of one minute each. The ultrasonic cycles (Branson 2510 ultrasonic bath, "set sonics" mode, power 60 W) produced nanosized objects within less than 15 min. For the preparation of nanoparticles from scallop-derived plasmalogens, four PEGylated dispersing agents (TPGS-PEG_{1000}, MO-PEG_{2000}, DSPE-PEG_{2000}, and Pluronic F167) were investigated with the purpose to find the conditions for steric stability of the formulations. The lipid concentration for the SAXS experiments was 10 wt.% with respect to the aqueous content. The stock lipid nanoparticle dispersions were diluted in an appropriate concentration range for cell culture experiments.

2.3. Quasi-Elastic Light Scattering (QELS)

The hydrodynamic diameters (d_h) of the particles in the investigated aqueous dispersions were determined by quasi-elastic light scattering (QELS) measurements using a Zetasizer Nano ZS90 apparatus (Malvern, France). The nanosizer instrument was equipped with a Helium−Neon laser of 633 nm wavelength. The particle samples were diluted to 0.5 wt.% lipid concentration prior to measurement in 1 cm thick cells and analyzed in an automatic mode using the following experimental parameters: temperature 25 °C; scattering angle, 90°; refracting index, 1.33; environment medium viscosity, 0.890 cP. Three measurements with the same cell were averaged for every sample. The results were analyzed using the MALVERN Zetasizer software and presented as statistic distribution plots of the particle hydrodynamic diameters. The average hydrodynamic diameter, d_h, was calculated considering the mean translational diffusion coefficient, D, of the particles in accordance with the Stokes–Einstein law for spherical particles in the absence of interactions, $d_h = k_B T/3\eta\pi D$, where k_B is the Boltzmann constant, T is temperature, and η is the viscosity of the aqueous medium. The plotted maximal intensities (in percentages) corresponded to the mean nanoparticle sizes, which were most abundant in the samples.

2.4. Synchrotron Small-Angle X-Ray Scattering (SAXS)

The dispersed nanoparticle samples were sealed in X-ray capillaries. The methodology of the performed SAXS measurements at the SWING beamline of synchrotron SOLEIL (Saint Aubin, France) was analogous to the previously described.[4] The samples were placed in a designed holder with (X,Y,Z) positioning. The temperature was 22 °C. The chosen sample-to-detector distance accounted for the soft matter sample properties. The X-ray beam spot size on the samples was 375×25 μm^2. The patterns were recorded with a 2D Eiger X 4 M detector (Dectris, Baden–Daettwil Switzerland) at 12 keV allowing measurements in the q-range from 0.0179 to 2.18 Å^{-1}. The q-vector was defined as $q = (4\pi / \lambda) \sin\theta$, where 2θ is the scattering angle. The synchrotron radiation wavelength was $\lambda = 1.033$ Å and the exposure time was 500 ms.

The synchrotron SOLEIL facility provides high-intensity, highly collimated, and monochromatic X-ray beams, resulting in excellent resolution and signal-to-noise ratio. The SWING beamline instrument was capable of achieving a resolution of up to 0.005 nm^{-1}. Given that our lipid nanoparticles have liquid crystalline structural organization, it was able to detect peak positions with a precision of 0.01 nm^{-1}. For the investigated soft matter samples, the calculated lattice parameters were reported with a precision of 0.1 nm^{-1}. The q-range calibration was done using a standard sample of silver behenate (d = 58.38 Å). An average of five spectra per sample was acquired. Data processing of the recorded 2D images was performed by the FOXTROT software as previously indicated.[4]

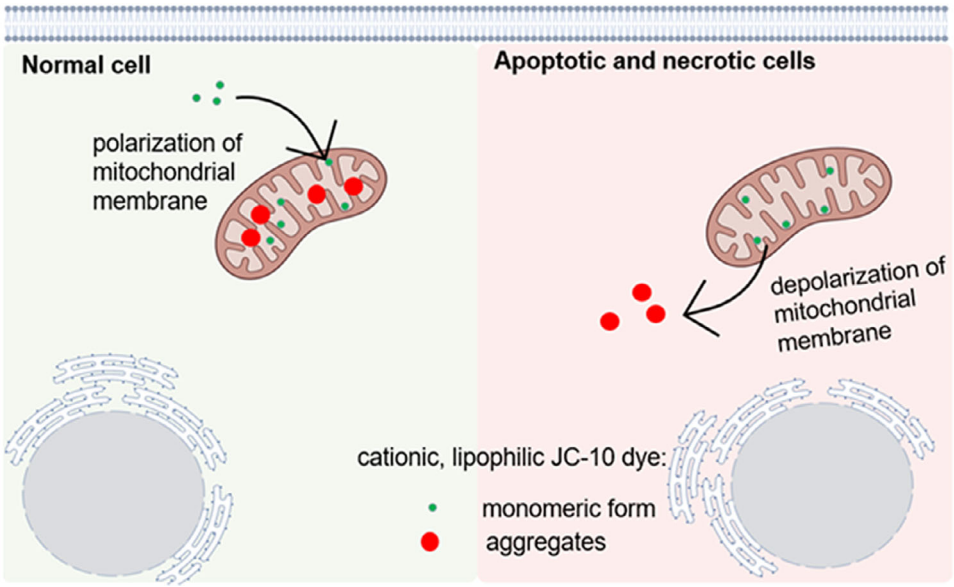

Figure 2. Schematic presentation of the principle of the mitochondrial membrane potential assay using a JC-10 dye. The employed lipophilic cationic fluorescent carbocyanine dye accumulates in mitochondria and forms J-aggregates characterized by red fluorescence (measured in the FL2 channel). Mitochondrial membrane depolarization (provoked by neurotoxicity or mitochondrial apoptosis) causes leakage of the monomeric green dye form from the mitochondria to the cytoplasm producing green fluorescence (measured in the FL1 channel). The experimental data were expressed as fluorescence intensity ratios [red (FL2)/green (FL1)], where the green fluorescence was recorded at the FL1 channel, while the red fluorescence was recorded at the FL2 channel. Created with BioRender (*BioRender.com*).

2.5. Antioxidant Assay

The antioxidant capacity of the investigated nanoparticles was determined by an Antioxidant Assay Kit (cat. No. MAK334, Sigma). The protocol included taking 20 µL of standards or samples and adding them to separate wells of a clear, flat-bottom 96-well plate. After that, 100 µL of Reaction Mix was added to all wells in the plates. Incubation was done for 10 min at room temperature. Once the incubation was done, the absorbance at 570 nm was measured with a microplate reader. The absorbance value of the blank (A570) was subtracted from those of all standard and sample A570 values. The result ΔA570 was plotted against the standard concentrations and the slope of the standard curve was determined. Finally, the Total Antioxidant Capacity (TAC) of every sample was calculated using the formula:

$$\mathrm{TAC}\,(\mu\mathrm{M}) = \frac{(\mathrm{A}_{570})_{\mathrm{sample}} - (\mathrm{A}_{570})_{\mathrm{blank}}}{\mathrm{Slope}\,(\mu\mathrm{M}^{-1})} \times \mathrm{n} \quad (1)$$

where $(A570)_{sample}$ denotes the absorbance of the sample, $(A570)_{blank}$ is the absorbance of the blank medium, and *n* is the sample dilution factor.

2.6. Cell Culture

The human neuroblastoma SH-SY5Y cell line was available from a previous work.[31] SH-SY5Y cells were grown in 75 cm^2 flasks with a complete Dulbecco's modified Eagles medium (DMEM) containing high glucose concentration (Sigma, France), 1% penicillin-streptomycin (Sigma), and 10% (v/v) FBS (Sigma). The cell culture was maintained in a humidified 5% CO_2 atmosphere at 37 °C. The SH-SY5Y cells were subcultured every 4 days with a 1:3 split ratio. Briefly, 3 mL trypsin (0.05% w/v)/EDTA (0.02% w/v) was employed for 5 min to detach the adherent cells after washing them with a sterile phosphate-buffered saline (PBS) deficient of calcium ions. Fresh complete medium DMEM (7 mL) was added to stop the trypsin reaction. The pellet was collected by ultracentrifugation at 200 rpm for 5 min and diluted by 10 mL fresh complete medium. For subsequent experiments, the SH-SY5Y cells were differentiated to a neuronal phenotype using 10 µM retinoic acid (RA) for 5 days. The differentiation was initiated at ≈70–80% cell confluence, on the second day of seeding, by replacing the culture medium with 15 mL fresh complete medium containing 10 µM RA. The cells investigated in this work were collected from passage numbers of less than 25.

2.7. Cellular Viability Determined by MTT Assay

The cellular viability was evaluated after incubation with the prepared plasmalogen-loaded nanoparticles. The viability was determined by the tetrazolium salt test (3-(4,5-dimethylthiazol-2-yl)-2,5-diphenyl tetrazolium bromide, MTT) after SH-SY5Y cell culture treatment by the studied nanoparticles. This assay was based on the conversion of the MTT reagent into formazan by the mitochondrial succinate dehydrogenase enzyme in the living cells. The MTT compound forms a purple insoluble precipitate, the amount of which was proportional to the metabolic activity of living cells. The cells were seeded at a density of 10 × 104 cells/well in 96-well plates. The culture medium was completely removed and replaced with a fresh complete medium containing

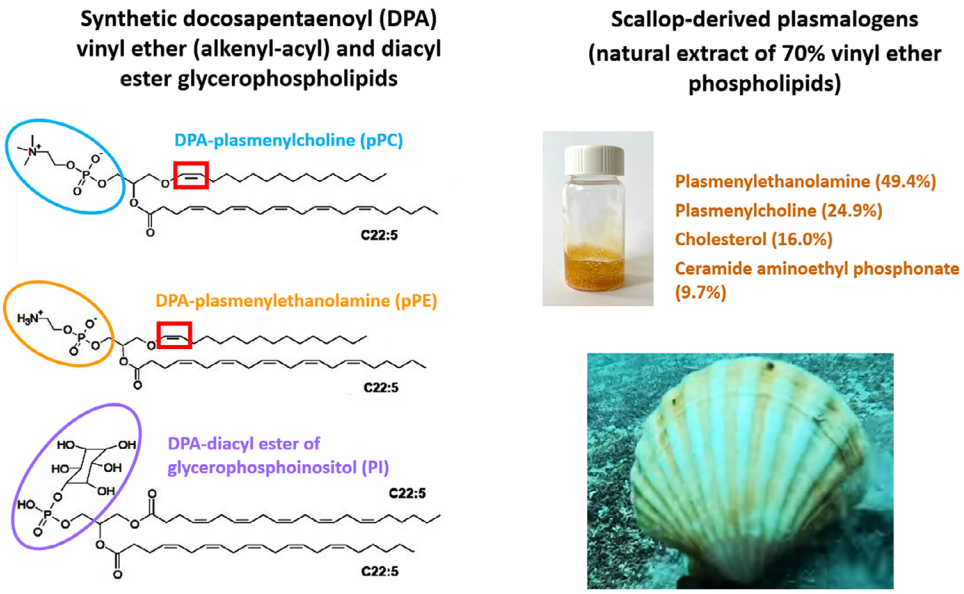

Figure 3. (Left) Chemical structures of synthetic phospholipids with polyunsaturated docosapentaenoyl (DPA) chains, which were custom prepared with high purity (>99%) for inclusion in liquid crystalline nanoparticles by self-assembly. From top to bottom: 1-O-1′-(Z)-hexadecenyl-2-(4Z,7Z,10Z,13Z,16Z-docosapentaenoyl)-sn-glycero-3-phosphocholine, C16:1p-22:5n6 PC (pPC) and 1-O-1′-(Z)-hexadecenyl-2-(4Z,7Z,10Z,13Z,16Z-docosapentaenoyl)-sn-glycero-3-phosphoethanolamine, C16:1p-22:5n6 PE (pPE), which are vinyl ether-type (1-alkyl-1′-enyl, 2-acyl) glycerophospholipids with phosphocholine (PC) and phosphoethanolamine headgroups (PE), and 1,2-bis(4Z,7Z,10Z,13Z,16Z-docosapentaenoyl)-sn-glycero-3-phosphoinositol, 22:5n6 PI (PI) (which is a lipid with two DPA chains that compensate the bulky phosphoinositol (PI) polar headgroup volume by an enriched double-chain hydrophobic volume). (Right) Photograph of a vial containing a natural lipid extract of scallop-derived plasmalogens (with 70% vinyl ether phospholipid content and small percentages of cholesterol and ceramide aminoethyl phosphonate (CAEP)).

RA (10 μM). The cells were maintained for differentiation at 37 °C in a humidified 5% CO_2 incubator. The RA-differentiated SH-SY5Y cells were deprived of FBS for 24 h and exposed to different nanoparticles with constant (or varying) concentrations for 24 or 48 h at 37 °C. Untreated, RA-differentiated SH-SY5Y cells were used as controls. The MTT solution with 5 mg mL^{-1} concentration was prepared in PBS and was filtered before use. Then, 20 μL MTT reagent (5 mg mL^{-1}) was added to each well. After 1 h incubation of the cells with the MTT solution at 37 °C, the medium was removed and 200 μL 100% DMSO was added to the wells in order to solubilize the crystalline formazan precipitate. The optical density of the samples was recorded at 570 nm wavelength by using a multiwell-scanning plate reader (LT-5000 MS, Labtech). The quantification was done by averaging the measurements of a minimum of six wells.

2.8. Flow Cytometry Analysis of Lipid Nanoparticle Internalization

The SH-SY5Y cells were cultured in 6-well plates at a density of 3×10^5 cells/well. After 5 days of differentiation by 10 μM retinoic acid, the cells were treated with nanoparticles labeled by a fluorescent lipid for different incubation times between 1 and 24 h. Then, the cells were washed three times by PBS and incubated with cell staining buffer (Cell Signaling) for 5 min. After detachment of the adherent cells, the cell suspension was transferred into an Eppendorf tube and ultracentrifuged at 200 rpm for 5 min. The pellet was separated from the supernatant and diluted in 1 mL PBS. The fluorescence of the samples was recorded in the FL2 channel of the flow cytometer BD Accuri C6 (Becton Dickinson).

2.9. Mitochondrial Membrane Potential Assay with a JC-10 Dye

Mitochondrial membrane potential changes ($\Delta\psi$) were probed by a JC-10 dye assay (Abcam, CA, USA). The SH-SY5Y cells were cultured in 6-well plates at the density of 3×10^5 cells/well. After 5 days of differentiation by 10 μM retinoic acid, the cells were treated with 10 μM lipid nanoparticle formulations for 24 h. Incubation with 5 μM trifluoromethoxy carbonylcyanide phenylhydrazone (FCCP) for 30 min was studied as a positive control. The untreated (RA-differentiated) cells were used as a negative control. The cells were stained by JC-10 dye for 15 min and protected from light. Washing with PBS (two times) and 0.5 mL Trypsin-EDTA solution was done in each well for detaching the cells. The cell suspension was transferred into an Eppendorf tube and ultracentrifuged at 200 rpm for 5 min. The pellet was separated from the supernatant and washed two times with PBS. The samples were measured using an Accuri C6 flow cytometer (Becton Dickinson). The green fluorescence was recorded at the FL1 channel, whereas the red fluorescence was recorded at the FL2 channel. The experimental data were expressed as fluorescence intensity ratios [red (FL2)/green (FL1)] representing the state of the JC-10 dye in the cells (**Figure 2**). The JC-10 dye was aggregated in normal cells, whereas the monomeric form was released when the MMP was decreased. The principle of the MMP measurement explores the equilibrium between the monomeric

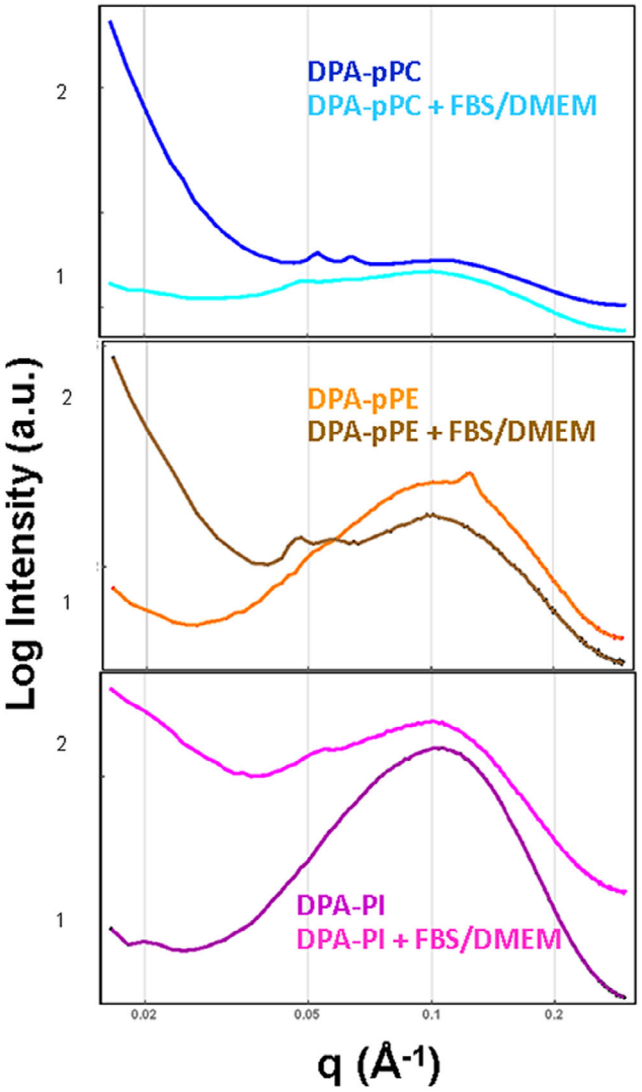

Figure 4. Synchrotron small-angle X-ray scattering (SAXS) patterns of liquid crystalline lipid nanoparticle dispersions embedding custom synthesized docosapentaenoyl glycerophospholipids (DPA-pPC, DPA-pPE, and DPA-PI) (see Table S1, Supporting Information for details of the formulations). The temperature is 22 °C. Aqueous phase composition (dark blue, orange, and dark purple lines): 1×10^{-2} M phosphate buffer containing butylated hydroxytoluene (BHT). The other SAXS plots (light blue, brown, and pink lines) were recorded after 48 h incubation of the nanocarriers with DMEM medium containing FBS.

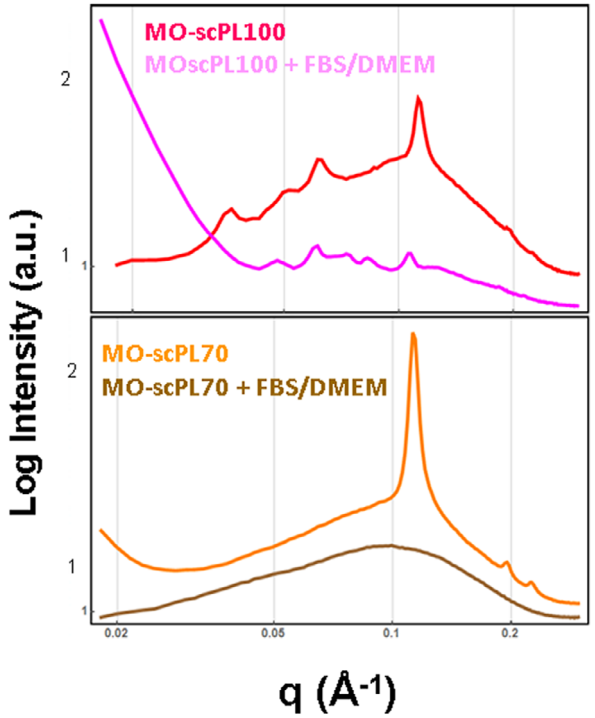

Figure 5. Synchrotron SAXS patterns of liquid crystalline lipid nanoparticle dispersions produced by self-assembled mixtures of scallop-derived plasmalogens scPL100 and scPL70 and MO (see Table S1, Supporting Information for the compositions of scPL100- and scPL70-based mixed assemblies). The temperature is 22 °C. Aqueous phase composition (red and orange lines): 1×10^{-2} M phosphate buffer containing butylated hydroxytoluene (BHT). The lower SAXS plots (pink and brown lines) were recorded after 48 h incubation of the nanocarriers with DMEM medium containing FBS.

form of the JC-10 dye (characterized by green fluorescence) and its J-aggregates (characterized by red fluorescence).

2.10. Apoptosis Analysis of Nanoparticle-Treated Cells by Flow Cytometry

The eventual induction of cellular apoptosis by lipid NPs (*e.g.*, MO-scPL70 sample) was studied by flow cytometry using the Annexin-V-FLUOS Staining Kit (Roche, cat. No. 11858777001). Briefly, SH-SY5Y cells were seeded at a density of 10^6 cells in 25 cm^2 culture flasks containing 5 mL of DMEM. After 24 h, the cell culture medium was replaced by 10 μM RA solution for 5 days of incubation. Then, lipid NPs (10 μM) were introduced in the FBS-free medium. After 24 h of incubation, the cells were washed with cold PBS and collected by trypsinization. The pelleted cells were resuspended in 100 μL of Annexin-V-FLUOS labeling solution and incubated at room temperature in dark for 10 min. The stained cells were analyzed on the BD C6 Accuri flow cytometer using the FL-1 channel (Ex. 488 nm/Em 530 nm) for detection of Annexin-V-FLUOS fluorescence and the FL-2 channel (Ex. 488nm/Em 578 nm) for the propidium iodide fluorescence. Incubation with 200 μM neurotoxin 6-OHDA for 30 min was used as a positive control.

2.11. Quantitative Determination of Caspase-3, Bax, and Bcl2 Activities

Caspase-3, Bax, and Bcl2 activities were assessed separately using commercially available Cell-Based ELISA kits. Caspase-3 activity was evaluated using the Caspase-3 (Human) Cell-Based ELISA kit (Abnova, cat. No. KA2637), Bax activity was evaluated using the BAX (Human) Cell-Based ELISA kit (Abnova, cat. No. KA2602), and Bcl2 activity was evaluated using the BCL2 (Human) Cell-Based ELISA kit (Abnova, cat. No. KA2604). The assays were conducted as per the manufacturer's instructions.

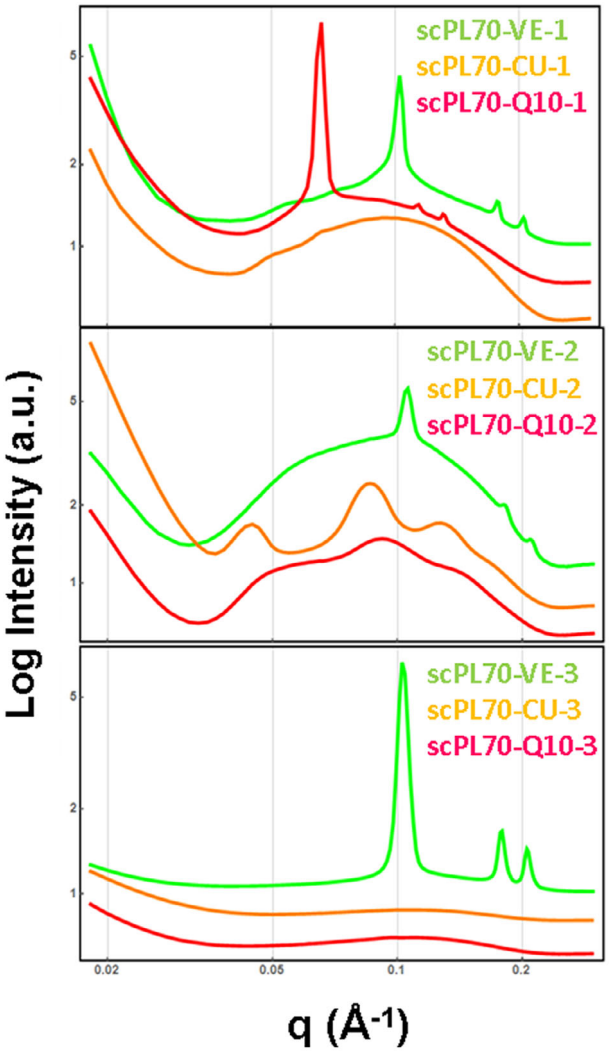

Figure 6. Synchrotron SAXS patterns of liquid crystalline lipid nanoparticles formulated with scallop-derived plasmalogens scPL70 and different dispersing agents TPGS-PEG$_{1000}$, MO-PEG$_{2000}$, DSPE-PEG$_{2000}$, or Pluronic F167 (see Table S1, Supporting Information for compositions of the scPL70-based mixed assemblies). The temperature is 22 °C.

Cells were seeded at a density of 3 × 10^4 cells/well in a 96-well plate after 5 days of RA differentiation. They were then exposed to 10 μM NPs for 24 h in RA-containing medium without FBS. After fixing and washing the cells, primary and secondary antibodies were added and incubated accordingly. Following substrate addition and reaction blockage, absorbance at 450 nm was measured using a microplate reader. Crystal violet was used for cell counting. The plate was washed and air-dried before adding crystal violet solution. The plate was washed again until no more color came off. Finally, SDS solution was added, incubated, and the absorbance at 595 nm was determined.

2.12. Quantitative Determination of BDNF Levels

The BDNF levels in lysates of nanoparticle-treated cells were measured by a commercial ELISA kit Human Free BDNF immunoassay (R&D Systems, Cat. No. DBD00). The ELISA experiment was performed according to the manufacturer's instructions. In short, the cells were seeded in a T75 flask at a density of 10×10^6 cells. On the second day, the medium was replaced with RA-containing complete medium. The medium was refreshed every three days. On the sixth day, the cells were incubated with 10 μM NPs in RA-containing medium without FBS for 24h. In the control group, the medium was changed to RA-containing medium without FBS. The cells underwent two washes with PBS, and then 1 mL of lysate buffer was added, followed by incubation on ice for 20 min. The resulting lysates were introduced to pre-coated plates and left to incubate for 1 h. Afterward, the plates were washed three times with a washing solution and exposed to a detection antibody for 1 h. Subsequently, the plates underwent another round of washing and were then incubated with streptavidin-HRP for 30 min. Finally, the plates were washed again and subjected to substrate/chromogen solution for development. The spectrophotometric measurements of absorbance at 450 nm were used to quantify the BDNF protein. The total protein concentration of the studied cell lysates was determined using a Bradford Reagent (B6916, Sigma).

2.13. Statistical Analysis

All the data presented were mean ± SEM. Analysis between the groups was carried out with one-way ANOVA (analysis of variance) with post hoc analysis by Tukey–Kramer multiple comparison method. Analysis between two groups was carried out with an unpaired *t*-test. Variation with $p < 0.05$ was significant.

3. Results and Discussion

3.1. Structural Characterization and Physico-Chemical Properties of the Lipid Nanoparticles

The investigated plasmalogen constituents for preparation of self-assembled lipid NPs are presented in **Figure 3**. They comprise i) synthetic docosapentaenoyl (DPA) plasmenyl (vinyl ether) and diacyl glycerophospholipids with phosphocholine (PC), phosphoethanolamine (PE), and phosphoinositol (PI) headgroups (with chemical structures designed based on a lipidomic analysis of mitochondrial membranes) (Figure 3, left panel), and ii) natural scallop-derived plasmalogens extract (Figure 3, right panel). The latter was available from previously performed clinical trials with AD patients.[54] The custom-synthesized DPA-plasmenyl lipids (Figure 3, left panel) and the scallop-derived plasmalogens were incorporated into amphiphilic assemblies, which were dispersed into nanoparticles. Liquid crystalline nanostructures were fabricated by self-assembly using amphiphilic mixtures of plasmalogens with the lyotropic lipid MO. This single-chain monoglyceride is suitable as a co-lipid for the generation of mixed nonlamellar nano-assemblies and NPs.[4,32]

3.1.1. Synchrotron SAXS Investigation of Nanoparticle Organizations and their Stability in Cell Culture Medium

Figures 4 to **6** show the synchrotron SAXS patterns acquired with the designed formulations of plasmalogen-based nanoparticles,

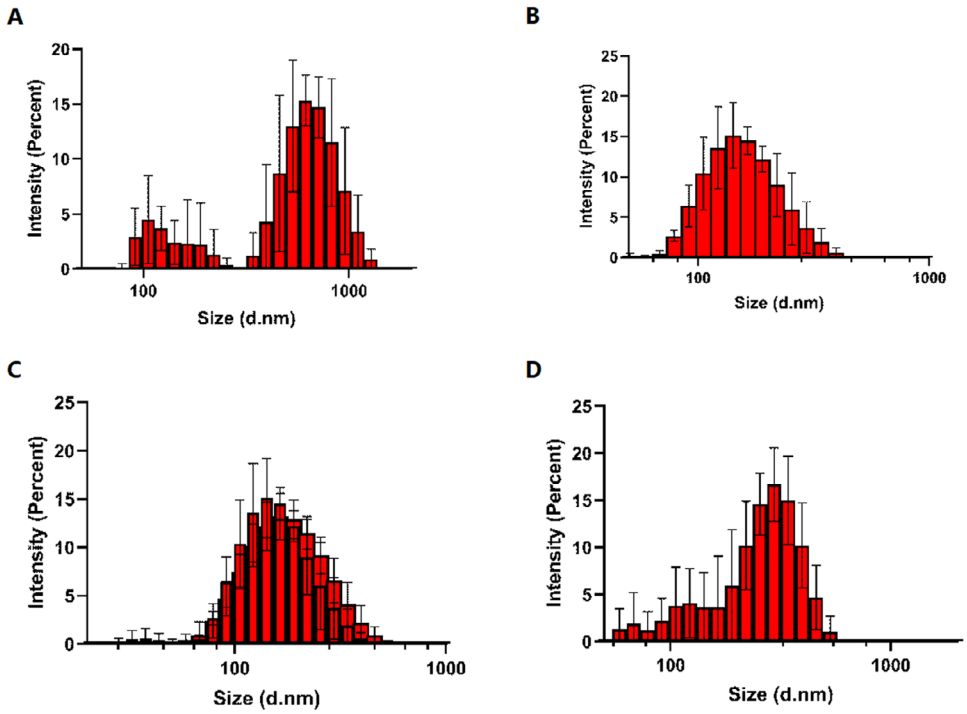

Figure 7. Nanoparticle size distributions determined by quasi-elastic light scattering measurements with formulations of scallop-derived plasmalogens: A) scPL70-VE-2, B) scPL70-VE-1, C) scPL70-CU-1, D) scPL70-CU-2.

which were dispersed in excess aqueous medium with the help of several biocompatible PEGylated dispersing agents (TPGS-PEG_{1000}, MO-PEG_{2000}, DSPE-PEG_{2000}, or Pluronic F167) (Table S1, Supporting Information). The lipid mesophase assemblies included small amounts of liposoluble antioxidants [vitamin E (VitE), curcumin (CU), or coenzyme Q_{10} (Q_{10})], which additionally stabilized the formulations of the synthetic and the scallop-derived (scPL100 and scPL70) vinyl-ether components. The determined liquid crystalline nanostructure type (topologies presented in Figure 1), and the corresponding lattice parameters are summarized in Table S1 (Supporting Information).

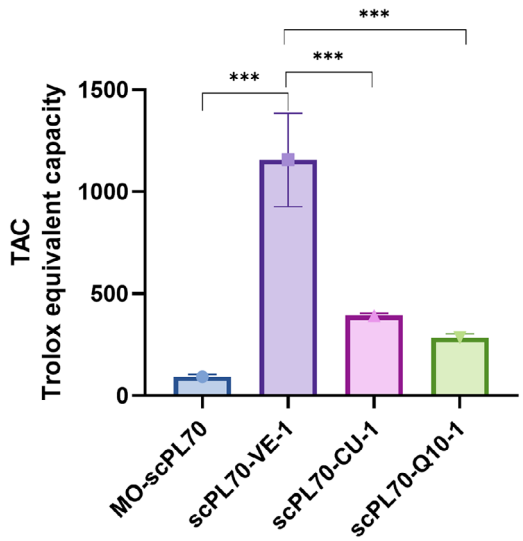

Figure 8. Total antioxidant capacity (TAC) of selected nanoformulations of scallop-derived plasmalogens listed in Table S1 (Supporting Information). The TAC is determined with Trolox as a standard compound. The concentration of the nanoparticles was 14 mM lipid content.

The self-assembly of the synthetic DPA-plasmenyl phospholipids with the lyotropic monoglyceride MO resulted in nonlamellar nanostructure formation as indicated in Figure 4. Structural features of coexisting cubosomes and vesicles were resolved in the SAXS pattern of the sample with encapsulated DPA-pPC plasmalogen (Figure 4, dark blue plot in the top panel). The q-vector positions of the Bragg peaks at $q_1 = 0.053$ Å^{-1} and $q_2 = 0.064$ Å^{-1} determined a unit cubic cell lattice parameter $a_{Q(Pn3\,m)} = 16.8$ nm for the dispersed cubosome particles. These peak positions belong to a sequence of Bragg diffraction peaks, spaced in the ratio $\sqrt{2} : \sqrt{3} : \sqrt{4} : \sqrt{6} : \sqrt{8}$ ..., which are characteristic of a bicontinuous cubic phase of the double diamond *Pn3 m* space group of symmetry.

A tendency for nonlamellar structure formation was established also in the SAXS pattern of the DPA-pPE plasmalogen nanocarriers (Figure 4, orange plot in the middle panel). The Bragg peak positioned at $q = 0.124$ Å^{-1} was attributed to the first Bragg peak of an inverted hexagonal H_{II} phase structure with a lattice parameter of $a_{HII} = 5.9$ nm. The inverted hexagonal (H_{II}) phase is characterized by a sequence of Bragg diffraction peaks with q-vector positions spaced in the ratio 1: $\sqrt{3} : \sqrt{4}$ .... Three peaks of a H_{II} phase structure were well resolved in Figures 5 and 6 below. The low intensity of the Bragg peak of the sample

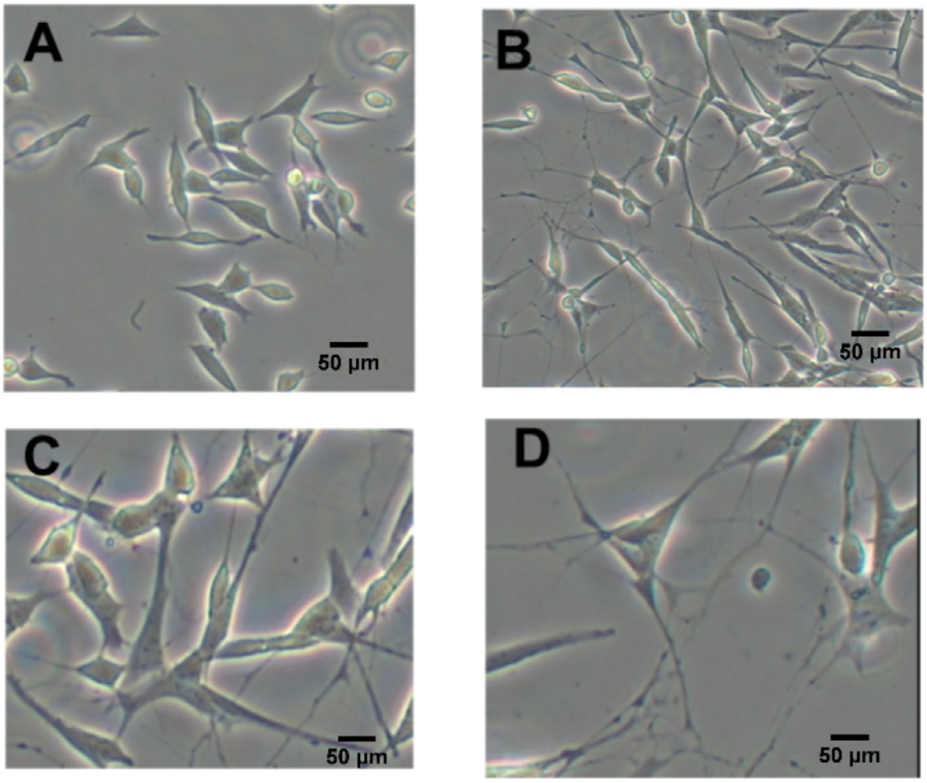

Figure 9. Optical micrographs illustrating the SH-SY5Y cellular confluence before and after 24 h treatment by lipid nanoparticulate formulations of DPA glycerophospholipids or scallop-derived plasmalogens at total lipid concentration of 10 µM. Conditions: A) Control SH-SY5Y cells differentiated by retinoic acid (RA) for 7 days in the absence of NPs, and 24 h incubation with B) scPL70-VE-1, C) scPL70-Q10-2, D) MO-scPL100 NPs (see the list of plasmalogen-based formulations in Table S1, Supporting Information).

presented in Figure 4 suggests that the hexosome particles involve a smaller number of periodically ordered H_{II} phase domains as compared to those presented in Figures 5 and 6 below.

The incorporation of DPA-PI, a double-chain phospholipid with PUFA chains, in the MO assemblies resulted in fluid membrane organization with no Bragg peaks of periodic nanostructures in the SAXS pattern (Figure 4, dark purple plot in the bottom panel). The broad maximum with a q-vector position at q_{max} = 0.101 Å^{-1} and the shoulder at smaller q-values correspond to lipid arrangement without periodicity, and that most likely comprises polydisperse vesicular membranes.

The nanoparticle (NP)-cell culture medium interaction and the nanocarrier stability on storage in cell culture medium were investigated by SAXS after 48 h incubation with DMEM medium containing FBS. The observed changes in the SAXS patterns in Figure 4 (light blue, brown, and pink lines) indicated that the curvature of the lipid membranes decreased upon nanocarrier incubation with DMEM/FBS media. This can be explained by the modification of the hydration and/or inner order of the lipid membrane assemblies as well as by the release of the docosapentaenoyl (DPA) glycerophospholipids (DPA-pPC, DPA-pPE, or DPA-PI) after 48 h incubation in the cell culture environment. A more significant change occurred in the DPA-pPE sample, for which a phase change from a hexosome NP structure (a_{HII} = 5.9 nm) to cubosome particles with large channels ($a_{Q(Pn3\,m)}$ = 19.3 nm) and vesicular membrane intermediates was deduced from the shift of the peak maxima (Figure 4, brown plot). It is suggested that the release of the PUFA plasmalogens (DPA-pPE and DPA-pPC) in the DMEM/FBS medium can perceptibly decrease the curvature of the host lipid membranes and lead to phase transitions in the formulations.

Figure 5 presents the SAXS patterns of nanoparticulate formulations prepared with the natural scallop-derived plasmalogens scPL100 and scPL70. At ambient temperature, two types of nonlamellar liquid crystalline structures were determined with the MO-scPL100 nanoparticulate assemblies, namely cubosome and hexosome structures (Figure 5, red plot in the upper panel). The q-vector positions of the Bragg peaks centered at q_1 = 0.036 Å^{-1}, q_2 = 0.051 Å^{-1} and q_3 = 0.062 Å^{-1} belong to a set of Bragg peaks spaced in the ratio $\sqrt{2} : \sqrt{4} : \sqrt{6} : \sqrt{8} : \sqrt{10} : \sqrt{12}$ ... They determine a primitive *Im3 m* cubic phase structure with a cubic unit cell lattice parameter $a_{Q(Im3\,m)}$ = 24.7 nm for the dispersed cubosome particles (MO-scPL100). The coexisting Bragg reflections at q_1 = 0.11 Å^{-1}, q_2 = 0.19 Å^{-1} and q_3 = 0.22 Å^{-1}, with q-vector positions spaced in the ratio 1: $\sqrt{3} : \sqrt{4}$, identified the formation of hexosome NPs with a unit cell lattice parameter a_{HII} = 6.6 nm.

For the MO-scPL70 nanoparticles, the positions of the three Bragg peaks at q_1 = 0.113 Å^{-1}, q_2 = 0.196 Å^{-1} and q_3 = 0.227 Å^{-1}, which are spaced in the ratio 1: $\sqrt{3} : \sqrt{4}$ (Figure 5, orange plot in the bottom panel), determined a lattice parameter a_{HII} = 6.4 nm for the inner inverted hexagonal (H_{II}) phase structure of the nanocarriers.

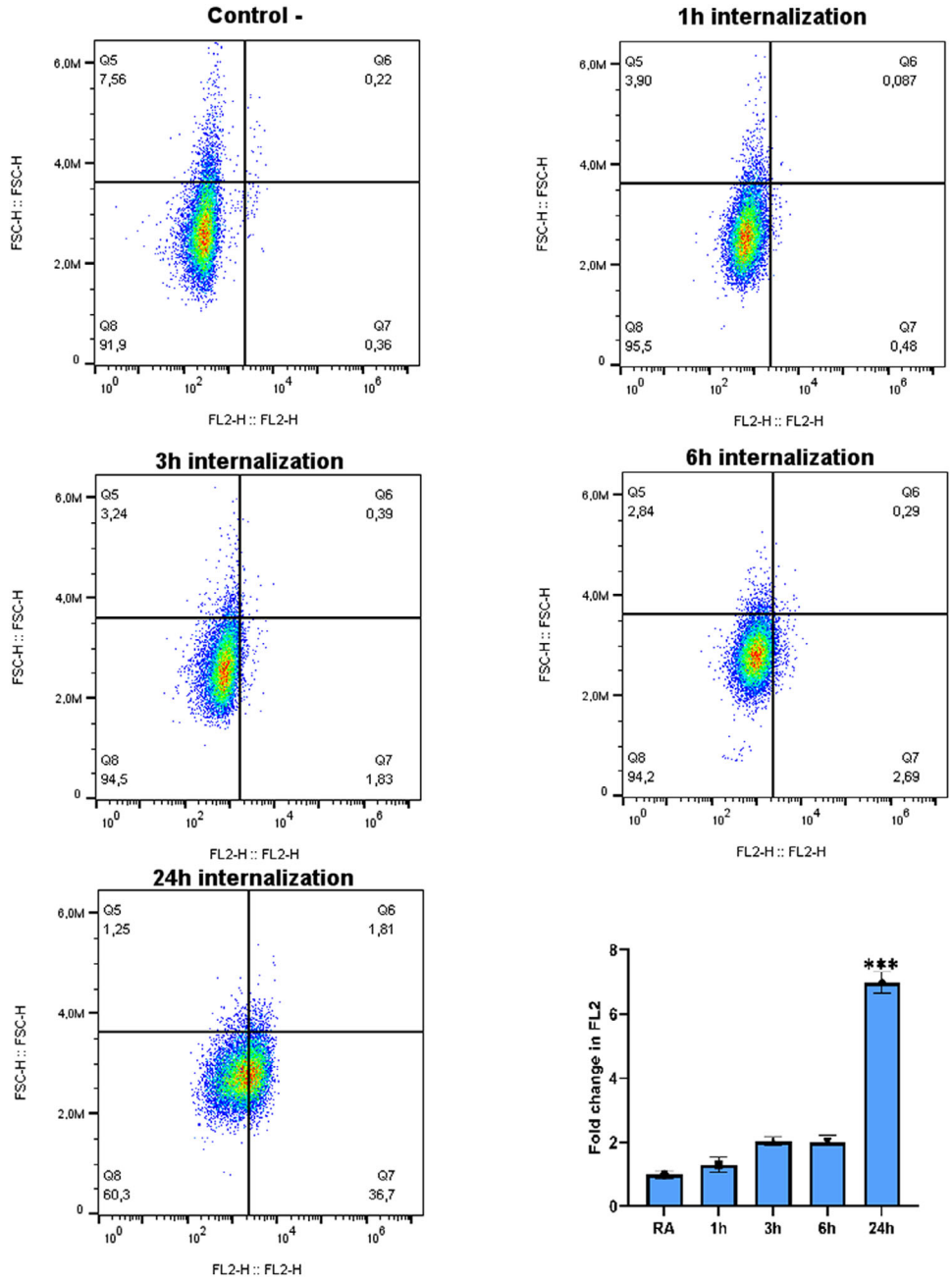

Figure 10. Liquid crystalline hexosome nanoparticle internalization kinetics monitored by flow cytometry measurements with respect to control differentiated SH-SY5Y cells (RA) at 1, 3, 6, and 24 h incubation with lipid nanoparticles labeled by 1 mol.% of fluorescent phospholipid 1,2-dioleoyl-sn-glycero-3-phosphoethanolamine-N-(lissamine rhodamine B sulfonyl) ammonium salt (18:1 Liss Rhod PE). The nanoparticle dispersion was with 10 μM total lipid concentration.

The SAXS patterns acquired after 48 h incubation of these nanocarriers with the DMEM/FBS medium established a topological transition associated with lipid membrane reorganization and interfacial lipid curvature decrease. Figure 5 (pink curve in the upper panel) indicates that the incubation with DMEM resulted in a coexistence of the cubic structure of the primitive space (*Im3 m*) space group with cubosomes of the diamond cubic (*Pm3 m*) space group, which is of lower membrane curvature. In parallel, the intensity of the Bragg peaks of the hexosomes considerably decreased (i.e., the DMEM medium increased the number of particles with decreased curvature). The lattice parameter of the coexisting particles, determined from the Bragg peak positions, are $a_{Q(Pn3\,m)}$ = 14.8 nm, $a_{Q(Im3\,m)}$ = 18.6 nm, and a_{HII} = 6.9 nm, respectively. The effect of incubation of the MO-scPL70 hexosome particles with DMEM/FBS medium resulted in disappearance of the periodic inner organization of the nanocarriers as revealed by Figure 5 (brown curve in the bottom panel; q_{max} = 0.097 Å^{-1}). This is also a manifestation of

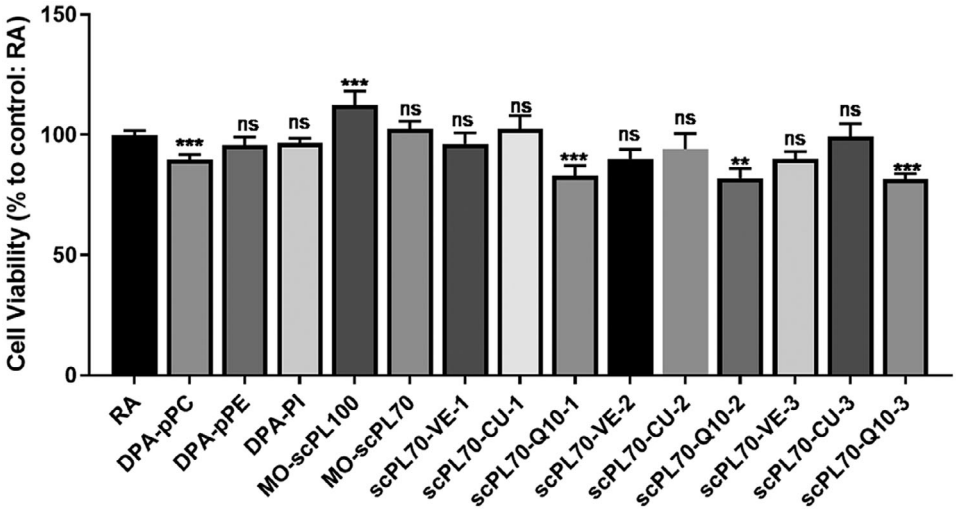

Figure 11. Cellular viability determined by a MTT assay with differentiated SH-SY5Y cells after 24 h of exposure to different formulations of plasmalogen-loaded NPs (listed in Table S1, Supporting Information) at the same total lipid concentration of 10 μM. The cells differentiated by retinoic acid (RA) for 7 days were considered as a control group with 100% viability. Differences were evaluated by one-way ANOVA. * $p \leq 0.05$, ** $p \leq 0.01$, and *** $p \leq 0.001$.

decreased interfacial lipid monolayer curvature and a transition from hexosomes to vesicular types of nano-objects.

The stability of the scallop-derived plasmalogen-based nanoparticles was controlled by co-lipid and PEGylated dispersing agent content. The effect of different PEGylated dispersing agents (TPGS-PEG_{1000}, MO-PEG_{2000}, DSPE-PEG_{2000}, or Pluronic F167) on the nanoscale organization of scallop-derived (scPL70) plasmalogen particles is presented by the SAXS patterns in Figure 6. The determined nanocarrier type and the structural parameters of the formulations stabilized by liposoluble antioxidants, e.g., vitamin E (VitE), curcumin (CU), or coenzyme Q_{10} (Q_{10}), are given in Table S1 (Supporting Information). The nonlamellar propensity of the scPL70-based mixtures was revealed by the formation of hexosome particles with inner inverted hexagonal (H_{II}) phase organization. For instance, the q-vector positions at $q_1 = 0.066$ Å^{-1}, $q_2 = 0.11$ Å^{-1} and $q_3 = 0.13$ Å^{-1} (which are spaced in the ratio 1: $\sqrt{3}$: $\sqrt{4}$) determined a lattice spacing $a_{HII} = 11.0$ nm for the scPL70-Q10-1 sample (Figure 5, red plot in the upper panel). The Bragg peak positions at $q_1 = 0.103$ Å^{-1}, $q_2 = 0.178$ Å^{-1}, and $q_3 = 0.206$ Å^{-1} determined a periodic structure with a lattice parameter $a_{HII} = 7.0$ nm for the scPL70-VE-3 inverted hexagonal (H_{II}) phase organization (Figure 6, green plot in the bottom panel).

Some scPL70-based formulations dispersed with the double-chain phospholipid DSPE-PEG_{2000} yielded oligo-lamellar vesicles with a repeat spacing d = 14.3 nm (Figure 6, orange plot in the middle panel).

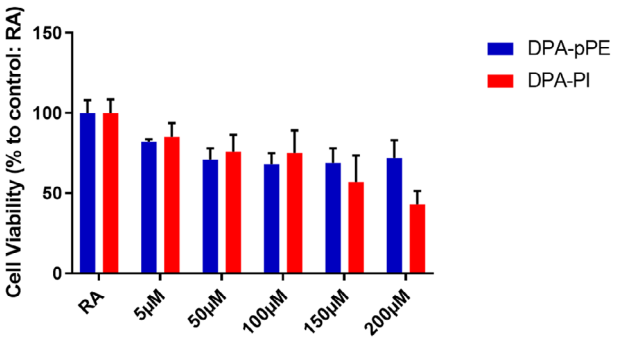

Figure 12. Dose-dependent plasmalogen nanoparticle effect on the viability of RA-differentiated SH-SY5Y cells determined by MTT test. The cells were treated for 24 h with increasing concentrations of DPA-pPE or DPA-PI loaded nanoparticles after 5 days of differentiation by retinoic acid (RA). The indicated concentrations (5–200 μM) refer to the total lipid concentration in the NP formulations. The cells differentiated by RA (10 μM) for 7 days were considered as a control group of 100% viability. Differences were evaluated by one-way ANOVA. * $p \leq 0.05$, ** $p \leq 0.01$, and *** $p \leq 0.001$.

3.1.2. Nanoparticle Size Distribution

Typical plots of hydrodynamic nanoparticle size distributions deduced from Malvern Zetasizer measurements are presented in **Figure** 7. The values of the mean hydrodynamic diameters, d_h, of the liquid crystalline NP dispersions embedding docosapentaenoyl (DPA) glycerophospholipids (DPA-pPC, DPA-pPE, and DPA-PI) or scallop-derived plasmalogens are given in Table S1 (Supporting Information). The results indicated the presence of two main populations of NPs in almost all dispersions produced by sonication. They are regarded as coexistences of small nanoparticles (vesicles) and larger particles (cubosomes, hexosomes or oligolamellar vesicles). The vesicular membranes, generated upon sonication and dispersion of the lipid mixtures, constitute reservoirs of membrane building blocks for the assembly of nonlamellar lipid particles.

Considering that the hexosomes are nanocarriers of an asymmetric shape, the approximation of the nanoparticle hydrodynamic diameter, d_h, by a diameter of a spherical object resulted in relatively big mean d_h values. The experimental data in Figure 7 confirm this finding. Thus, large nanoparticle sizes (mean $d_h \approx$ 500–600 nm) dominated the size distribution of the nonlamellar hexosome NPs (Table S1, Supporting Information).

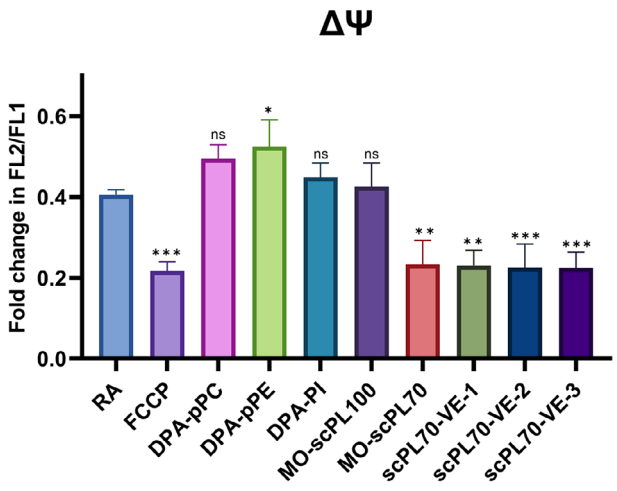

Figure 13. Determination of mitochondrial membrane potential (MMP) changes ($\Delta\psi$) by flow cytometry analysis using a JC-10 dye probe. Histograms of the fluorescence intensity ratio FL2/FL1 for control SH-SY5Y cells (RA), cells incubated with 5 µM FCCP dissolved in ethanol (positive control), or nanoparticle formulations with 10 µM total lipid concentration. The investigated nanoparticulate formulations are described in Table S1 (Supporting Information).

The diversity of the structures established by SAXS is consistent with the NP topologies and nano-object coexistences observed by cryo-TEM imaging. Figure S1 (Supporting Information) reveals that the existing structural polymorphism of the plasmalogen-based mixtures[33] enables the fabrication of either nonlamellar nanoparticles or mixed objects and vesicular membranes. The morphological examination confirmed the liquid crystalline nanocarrier structure types. The self-assembly technique yielded plasmalogen-based nanoassemblies of hexosome, cubosome, vesicular or intermediate types of topologies. It was of interest to investigate the interaction of these different kinds of particles with living cells of neuronal phenotype such as the differentiated human neuroblastoma SH-SY5Y cells.

3.2. Total Antioxidant Capacity of Plasmalogen-Based Nanoparticles

We further investigated the effect of the plasmalogen-based mixed compositions on the in vitro antioxidant capacity of the aqueous nanoparticulate dispersions. Nanoformulations of the natural plasmalogen scPL70 extract, containing equal quantities of plasmalogen (scPL70-VE-1, scPL70-CU-1, and scPL70-Q10-1), were compared in a total antioxidant capacity (TAC) assay. The determined TAC of the nanoparticles are shown in **Figure 8**. At constant plasmalogen content, the scPL70-VE-1 nanoparticles, containing VitE, exhibited higher antioxidant capacity than those encapsulating curcumin or coenzyme Q_{10} in the mixtures. This result suggested synergistic antioxidant effects of scPL70 and VitE, which present interest for further investigations.

In the next step, we investigated the interaction of nanoparticles of different kinds of topologies, established by the synchrotron SAXS analyses (Figures 4, 5, and 6), with living cells of a neuronal phenotype such as the differentiated human neuroblastoma SH-SY5Y cells. In general, liquid crystalline nanoparticles of nonlamellar lipids are suitable for improving the bioavailability of challenging compounds involving PUFA chains.[4,32] Various nanoparticulate formulations have been developed for encapsulation of neuroprotective compounds for central nervous system (CNS) targeting.[57–63] In a comparative previous study, cubosome and hexosome liquid crystalline lipid particles, characterized by different inner nanochannel organizations, have provided essentially different brain concentrations of phenytoin (an anti-seizure drug) after in vivo NP-mediated drug administration.[25] In this work, the viability of neuronal cells incubated with the liquid crystalline nanoparticles, loaded with DPA glycerophospholipids (DPA-pPC, DPA-pPE, and DPA-PI) or natural plasmalogens (scPL70), was studied by optical microscopy and an MTT assay.

3.3. SH-SY5Y Cellular Morphology after Treatment by Plasmalogen-Based Lipid Nanoparticles

The cellular confluence of differentiated SH-SY5Y cells was monitored by optical micrographs before and after nanoparticle treatment (**Figure 9**). The differentiated cells were exposed to formulations of NPs with 10 µM total lipid concentration. Generally, the cellular confluence did not decrease after 24 h incubation with plasmalogen-loaded NPs. The observed neurite outgrowth was consistent with the neuronal cell phenotype.

3.3.1. Cellular Uptake of Lipid Nanoparticles Determined by Flow Cytometry

A Rhodamine B dye-labeled phospholipid was included in the studied hexosome lipid nanoparticles to follow their uptake into differentiated SH-SY5Y cells by flow cytometry analysis. The internalization kinetics of the lipid NPs was probed by the time evolution of the fluorescence intensities in the quadrants shown in **Figure 10**. The histograms in Figure 10 indicate that the NPs were internalized more considerably after 3 h of cellular incubation and produced significant intracellular fluorescence after 24 h.

3.4. Cellular Viability after Incubation with Plasmalogen-Based Lipid Nanoparticles

The SH-SY5Y cellular viability was quantified by an MTT assay (**Figure 11**). The obtained data represent the mitochondrial activity in the cells and indicate that the plasmalogen-loaded particles are non-toxic to the differentiated human cells at 10 µM total lipid concentration. The observed cellular confluence in Figure 9 is in accordance with these MTT results.

To study the dose-response, the differentiated SH-SY5Y cells were exposed to DPA-phospholipid encapsulating NPs with increasing concentrations up to 200 µM (**Figure 12**). The results of the performed 24 h MTT test indicated that the viability decreases more significantly at total lipid concentration above 100 µM. For the given example of high lipid concentrations of the formulations, the SH-SY5Y cellular viability was superior after incubation with vinyl-ether lipid (DPA-pPE)-loaded NPs as compared to the diacyl glycerophospholipid (DPA-PI)-loaded nanoparticles.

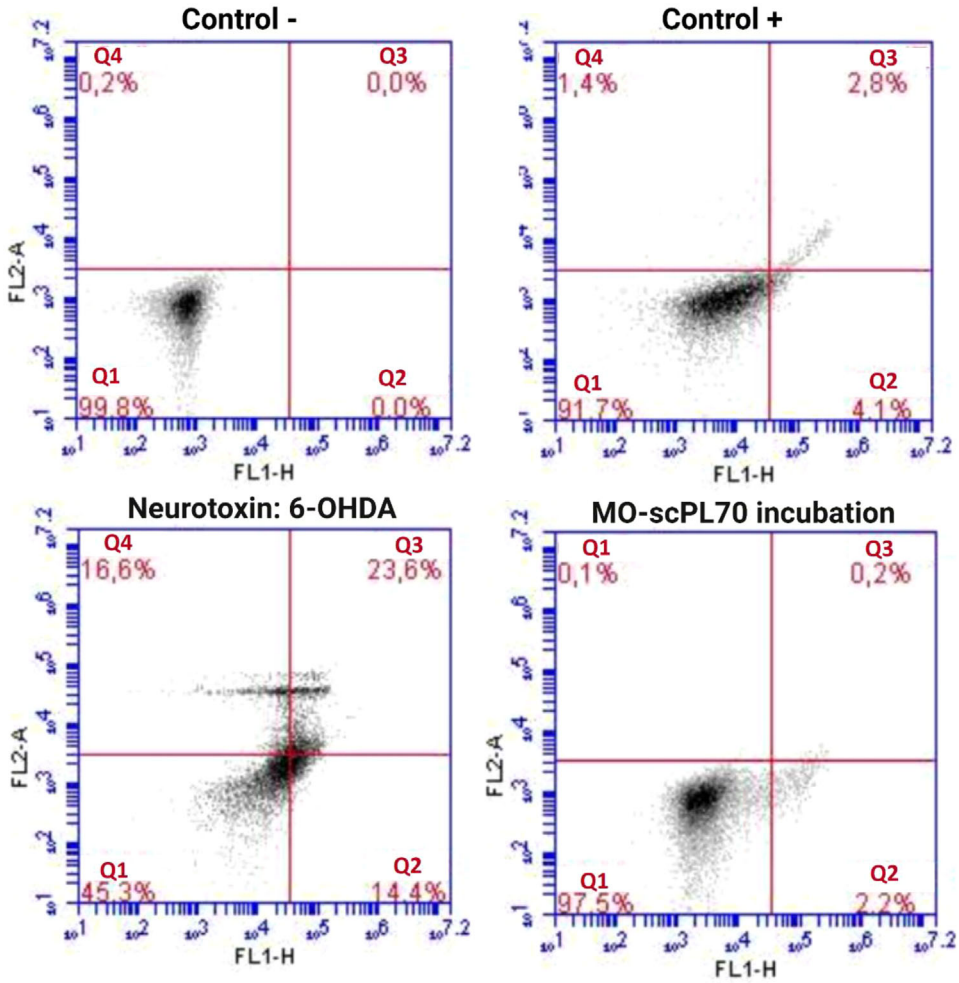

Figure 14. Flow cytometry apoptosis assay analysis determining RA-differentiated live, apoptotic, and necrotic (dead) SH-SY5Y cells after staining with Annexin-V-FLUOS and propidium iodide. For each sample, 10.000 cells were analyzed, and a quadrant analysis was performed to determine the proportions (%) of cells in each quadrant: Q1 represented living cells, Q2 represented apoptotic cells, and Q3 represented necrotic cells. The assay was conducted following a 24 h treatment of RA-differentiated SH-SY5Y cells with plasmalogen-loaded NPs. The control (−) group consisted of RA-differentiated SH-SY5Y cells without staining, while the control (+) group consisted of RA-differentiated SH-SY5Y cells stained with Annexin-V-FLUOS and propidium iodide. Incubation with the neurotoxin 6-OHDA was used as a positive control.[64]

3.5. Mitochondrial Membrane Potential Changes

The depolarization of the mitochondrial membranes of the cells and the changes in MMP ($\Delta\psi$), due to treatment by plasmalogen-based nanoparticles, were probed with the JC-10 dye. The results of the performed flow cytometry determination of the MMP changes are shown in **Figure 13**. The differentiated SH-SY5Y cells were incubated with 10 µM nanoparticle formulations and the fluorescence intensities ratios [red (FL2)/green (FL1)] were compared for the nanoparticle-treated conditions versus the non-treated cells (RA) and the positive control sample (FCCP). The histograms in Figure 13 revealed that the MMP changes are distinguishable for two groups of nanoformulations: i) synthetic DPA-phospholipid NPs, which do not notably influence MMP, and ii) natural scallop-derived plasmalogen-based NPs, which influence MMP.

Figure 13 shows also that no essential differences in the FL2/FL1 ratios occur among the compositions involving the natural scallop-derived plasmalogens. Therefore, the investigated amphiphilic compositions influenced more essentially the structural organization of the self-assembled plasmalogen-loaded particles but have had similar effects on the cellular viability and the MMP changes ($\Delta\psi$).

3.6. Apoptosis Assay Evidencing the Safety of Plasmalogen-Loaded Nanoparticles

The performed apoptosis assay demonstrated that the investigated plasmalogen-based nanoformulations are non-toxic. **Figure 14** shows that the exposure of neuronally-derived SH-SY5Y cells to plasmalogen-loaded NPs did not trigger apoptosis as compared to the positive control group that was induced with the neurotoxin 6-OHDA. The results revealed that 97.5% of cells treated with plasmalogen-loaded NPs remained viable, with only 2% showing signs of apoptosis (Figure 14). In contrast,

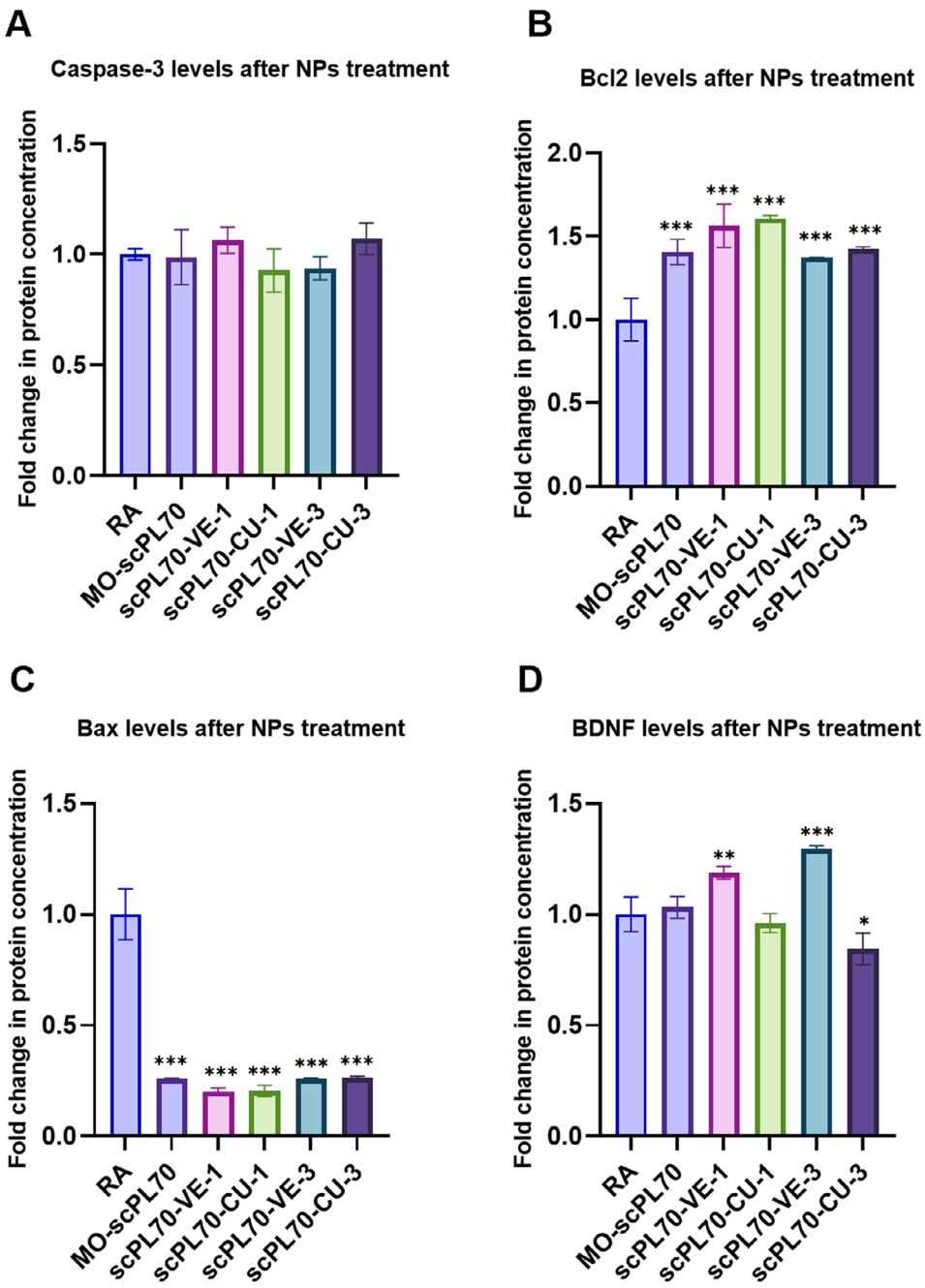

Figure 15. Results from ELISA assays showing the fold changes in caspase-3 activity, Bcl2 and Bax levels, and BDNF protein expression determined after 24 h incubation of different plasmalogen-based nanoparticles with RA-differentiated SH-SY5Y cells. The control group consisted of RA-differentiated SH-SY5Y cells subjected to 10 μM RA incubation for 5 days followed by 24 h deprivation of serum.

the control group treated with RA-containing DMEM without serum had an apoptotic population of 4.1%, likely due to starvation during the 24h incubation period. In fact, serum provides optimal conditions for cell growth and its deprivation induces cell apoptosis. Of note, the neurotoxin-treated (200 μM 6-OHDA) group was characterized by increased percentages of both apoptotic cells (from 4% to 14%) and necrotic cells (from 2.8% to 23.6%), thus leading to an essential decrease in the living cells population. These results imply that plasmalogen-loaded NPs did not induce cellular apoptosis under the investigated conditions.

3.7. Quantitative Determination of Protein Biomarkers after Cellular Treatment by Plasmalogen-Loaded Nanoparticles

Measurements of caspase-3, Bcl2, and Bax protein levels were done by cell-based ELISA. These proteins play a crucial role in

maintaining normal neuronal function.[65] Caspase-3 and Bax are crucial apoptotic proteins. **Figure 15A** shows that the examined plasmalogen-loaded NP formulations did not induce changes in the caspase-3 levels. Bax and Bcl2 play distinct roles in the cells: Bcl2 promotes cell survival by inhibiting apoptosis, while Bax accelerates cell death by promoting apoptosis. The results obtained in this work indicate that Bcl2 was upregulated by all NPs formulations, whereas Bax was downregulated (Figure 15B,C). Thus, these data evidenced the anti-apoptotic effect of the plasmalogen-loaded NPs.

Furthermore, the plasmalogen nanoformulations containing VitE exhibited a significant improvement in BDNF protein expression (Figure 15D). Under the investigated conditions (nanoparticle concentration and incubation time), other formulations did not provoke notable increase and, in some cases, even decreased the expression of BDNF. This data suggested that the nanocarrier type, as determined by the lipid composition, may influence the regulation of the protein biomarkers involved in neuronal cell survival and functional maintenance. In addition, the results revealed the potential of these formulations as neuroprotective drug delivery systems.

Recent work has hypothesized that the neuroprotection by plasmalogens can be mediated by neurotrophic signaling pathways such as the BDNF/TrkB-MAPK/AkT/PI-3K pathway.[42] In perspective, it would be therefore of interest to investigate the neuroprotective and neuro-restorative effects of the plasmalogen-loaded NPs in other models of neurodegeneration.

4. Conclusion

Lipid-based drug delivery nanosystems have opened innovative directions in nanomedicine development against neurodegenerative diseases. The use of plasmalogens in nanomedicine is at an emerging stage. Here natural scallop-derived plasmalogens were formulated in NPs in view of therapeutic delivery. Plasmalogens are vinyl ether glycerophospholipids, which can act as potent agents against aging and neurodegeneration thanks to their antioxidant properties and role in neuronal membranes. However, the bioavailability of these compounds needs to be improved for applications in nanomedicine. Nanocarrier formulations permit overcoming the stability problems of the plasmenyl vinyl ether phospholipids and improving their drug delivery properties. Similarly, to other phospholipids, the vinyl ether lipids (plasmalogens) display structural polymorphism. A remarkable propensity for nonlamellar phase formation has been noted in relation to supramolecular packing requirements.[66–69]

In the present work, a nonlamellar helper lipid excipient (MO) was used for nanoparticle structural stabilization of synthetic plasmalogens with polyunsaturated chains. It was possible to formulate the scallop-derived plasmalogens with or without MO. Different PEGylated amphiphiles were used for steric stabilization of the dispersed nanoparticles. The performed structural investigations established various structural features demonstrating the formation of cubosome and hexosome NPs as well as of vesicular membranes with different topologies. Hexosome and oligo-lamellar vesicle delivery systems of scallop-derived plasmalogens were stabilized by the inclusion of PEGylated shells and small amounts of vitamin E, curcumin, or coenzyme Q_{10}. The cellular viability study indicated that the obtained particles were non-toxic to human SH-SY5Y cells at a total lipid concentration of 10 μM. Cellular incubation with nanoparticles loaded by scallop-derived plasmalogens more significantly influenced the mitochondrial membrane potential (MMP) as compared to nanoparticles loaded by synthetic DPA-plasmalogens. The established synergistic antioxidant effects of scPL70 and VitE presented interest for further investigations. In perspective, it will be of interest to examine the interaction of the nonlamellar nanoparticles with phospholipid membranes as well as the relationship between the NP type and their antioxidant and neuroprotective properties in neurodegenerative disease models. Moreover, the observed increase in BDNF expression indicated a stimulating effect on neuronal health, which may help enhance synaptic plasticity and potentially influence cognitive function and mood regulation in therapeutic applications.

Supporting Information

Supporting Information is available from the Wiley Online Library or from the author.

Acknowledgements

Y.W. acknowledges a PhD fellowship from MESRI (France) and thanks Mélanie Hery and Dr. Juliette Vergnaud for helpful advice at the cell culture facility. A.A. and B.A. acknowledge collaboration with Dr. Markus Drechsler, and the allocated beamtime at Synchrotron SOLEIL (Saint Aubin, France) through the projects 20230326, 20210580, and 20201321 with all scientific and technical support at SWING beamline. B.A. was supported by the project "Structural Dynamics of Biomolecular Systems" (ELIBIO) (CZ.02.1.01/0.0/0.0/15_003/0000447). A.A. acknowledges membership in the CNRS GDR2088 BIOMIM research network. The scheme in Figure 2 was generated with BioRender (*BioRender.com*). The performed research was funded by the projects "Structural Dynamics of Biomolecular Systems" (ELIBIO) (CZ.02.1.01/0.0/0.0/15_003/0000447) and "Advanced research using high-intensity laser produced photons and particles" (CZ.02.1.01/0.0/0.0/16_019/0000789) from the European Regional Development Fund. Y.D. was supported by grants from the Wenzhou Institute, University of Chinese Academy of Sciences (Grant No. WIUCASQD2019005) and the National Natural Science Foundation of China (Grant No: 31 670 841).

Conflict of Interest

The authors declare no conflict of interest.

Author Contributions

Y.W. performed investigation, methodology, data processing, wrote the original draft. B.A. performed investigation, data analysis, data visualization, resources, wrote, review and edited the final manuscript. Y.D. performed synthetic plasmalogen lipids conception and management, resources. T.F. provided natural plasmalogens, materials and resources. M.S.H. provided natural plasmalogens, materials, and resources. T.B. performed instrument management, hardware, data visualization. A.A. performed conceptualization, investigation, experimental design and methodology, formal analysis, supervision, wrote the original draft, wrote, review and edited the final manuscript. All authors agree to be accountable for the content of the work.

Data Availability Statement

The data that support the findings of this study are available from the corresponding author upon reasonable request.

Keywords

cubosomes, hexosomes, lipid nanoparticles, nanotherapeutic assemblies, scallop-derived plasmalogens, synchrotron small-angle X-ray scattering

Received: March 3, 2024
Revised: August 31, 2024
Published online:

[1] M. Ahmed, U. Khan, A. Haye, N. Agarwal, N. Alhakamy, H. Alhadrami, M. Warsi, G. Jain, *Pharmaceuticals* **2020**, *13*, 356.
[2] A. M. Mohsen, M. M. Younis, A. Salama, A. B. Darwish, *J. Pharm. Sci.* **2021**, *110*, 2677.
[3] M. Rakotoarisoa, B. Angelov, V. M. Garamus, A. Angelova, *ACS Omega* **2019**, *4*, 3061.
[4] M. Rakotoarisoa, B. Angelov, S. Espinoza, K. Khakurel, T. Bizien, M. Drechsler, A. Angelova, *ACS Sustainable Chem. Eng.* **2021**, *9*, 14821.
[5] D. Lombardo, M. A. Kiselev, M. T. Caccamo, *J. Nanomater.* **2019**, *2019*, e3702518.
[6] L. Schoenmaker, D. Witzigmann, J. A. Kulkarni, R. Verbeke, G. Kersten, W. Jiskoot, D. J. A. Crommelin, *Int. J. Pharm.* **2021**, *601*, 120586.
[7] S. S. Nogueira, A. Schlegel, K. Maxeiner, B. Weber, M. Barz, M. A. Schroer, C. E. Blanchet, D. I. Svergun, S. Ramishetti, D. Peer, P. Langguth, U. Sahin, H. Haas, *ACS Appl. Nano Mater.* **2020**, *3*, 10634.
[8] J. A. Kulkarni, S. B. Thomson, J. Zaifman, J. Leung, P. K. Wagner, A. Hill, Y. Y. C. Tam, P. R. Cullis, T. L. Petkau, B. R. Leavitt, *Nanoscale* **2020**, *12*, 23959.
[9] B. Angelov, V. M. Garamus, M. Drechsler, A. Angelova, *J. Mol. Liq.* **2017**, *235*, 83.
[10] A. Angelova, M. Drechsler, V. M. Garamus, B. Angelov, *ChemNanoMat* **2019**, *5*, 1381.
[11] H. Liu, M. Bu, J. Tang, Y. Wei, Y. Sun, X. Wang, L. Wu, *IJN* **2015**, 6879.
[12] H. Yu, A. Angelova, B. Angelov, B. Dyett, L. Matthews, Y. Zhang, M. El Mohamad, X. Cai, S. Valimehr, C. J. Drummond, J. Zhai, *Angew. Chem., Int. Ed.* **2023**, *135*, e202304977.
[13] T. M. Allen, P. R. Cullis, *Adv. Drug Delivery Rev.* **2013**, *65*, 36.
[14] D. B. Fenske, P. R. Cullis, *Expert Opinion on Drug Delivery* **2008**, *5*, 25.
[15] D. Sanver, A. Sadeghpour, M. Rappolt, F. Di Meo, P. Trouillas, *Langmuir* **2020**, *36*, 11776.
[16] A. Yaghmur, H. Mu, *Acta Pharm. Sin. B* **2021**, *11*, 871.
[17] C. Tan, S. F. Hosseini, S. M. Jafari, *J. Agric. Food Chem.* **2022**, *70*, 1423.
[18] M. Fornasier, S. Biffi, B. Bortot, P. Macor, A. Manhart, F. R. Wurm, S. Murgia, *J. Colloid Interface Sci.* **2020**, *580*, 286.
[19] J. Zhai, B. Fan, S. H. Thang, C. J. Drummond, *Molecules* **2021**, *26*, 3648.
[20] Y. Li, A. Angelova, F. Hu, V. M. Garamus, C. Peng, N. Li, J. Liu, D. Liu, A. Zou, *Langmuir* **2019**, *35*, 14532.
[21] S. Murgia, A. M. Falchi, M. Mano, S. Lampis, R. Angius, A. M. Carnerup, J. Schmidt, G. Diaz, M. Giacca, Y. Talmon, M. Monduzzi, *J. Phys. Chem. B* **2010**, *114*, 3518.
[22] C. V. Kulkarni, V. K. Vishwapathi, A. Quarshie, Z. Moinuddin, J. Page, P. Kendrekar, S. S. Mashele, *Langmuir* **2017**, *33*, 9907.
[23] A. Angelova, B. Angelov, V. M. Garamus, M. Drechsler, *J. Mol. Liq.* **2019**, *279*, 518.
[24] H. M. Abdel-Bar, S. E. Khater, D. M. Ghorab, A. M. Al-mahallawi, *ACS Omega* **2020**, *5*, 26697.
[25] Y. Mohammad, R. N. Prentice, B. J. Boyd, S. B. Rizwan, *J. Colloid Interface Sci.* **2022**, *605*, 146.
[26] R. Prajapati, S. W. Larsen, A. Yaghmur, *Phys. Chem. Chem. Phys.* **2019**, *21*, 15142.
[27] M. M. Gabr, S. M. Mortada, M. A. Sallam, *J. Pharm. Sci.* **2017**, *106*, 3103.
[28] T. Qiu, P. Gu, A. Wusiman, H. Ni, S. Xu, Y. Zhang, T. Zhu, J. He, Z. Liu, Y. Hu, J. Liu, D. Wang, *Colloids Surf B Biointerfaces* **2021**, *204*, 111799.
[29] A. Yaghmur, B. V. Tran, S. M. Moghimi, *Molecules* **2019**, *25*, 16.
[30] A. Angelova, B. Angelov, *Neural Regen Res* **2017**, *12*, 886.
[31] M. Rakotoarisoa, B. Angelov, S. Espinoza, K. Khakurel, T. Bizien, A. Angelova, *Molecules* **2019**, *24*, 3058.
[32] A. Angelova, M. Drechsler, V. M. Garamus, B. Angelov, *ACS Omega* **2018**, *3*, 3235.
[33] A. Angelova, B. Angelov, M. Drechsler, T. Bizien, Y. E. Gorshkova, Y. Deng, *Front. Cell Develop. Biol.* **2021**, *9*, 617984.
[34] F. Dorninger, S. Forss-Petter, I. Wimmer, J. Berger, *Neurobiol. Disease* **2020**, *145*, 105061.
[35] P. Rong, J.-L. Wang, A. Angelova, Z. A. Almsherqi, Y. Deng, *Front. Cel Develop. Biol.* **2022**, 10, 859421.
[36] N. E. Braverman, A. B. Moser, *Biochimica et Biophysica Acta (BBA) – Molecular Basis of Disease* **2012**, *1822*, 1442.
[37] H. Che, L. Zhang, L. Ding, W. Xie, X. Jiang, C. Xue, T. Zhang, Y. Wang, *Food Funct.* **2020**, *11*, 1729.
[38] L. Kuerschner, D. Richter, H. K. Hannibal-Bach, A. Gaebler, A. Shevchenko, C. S. Ejsing, C. Thiele, *PLoS One* **2012**, *7*, e31342.
[39] D. Hahnel, K. Beyer, B. Engelmann, *Free Radic. Biol. Med.* **1999**, *27*, 1087.
[40] H. Che, Q. Li, T. Zhang, L. Ding, L. Zhang, H. Shi, T. Yanagita, C. Xue, Y. Chang, Y. Wang, *Food Funct.* **2018**, *9*, 3008.
[41] M.d. S. Hossain, M. Ifuku, S. Take, J. Kawamura, K. Miake, T. Katafuchi, *PLoS One* **2013**, *8*, e83508.
[42] M.d. S. Hossain, S. Mawatari, T. Fujino, *Front. Cell Develop. Biol.* **2022**, *10*, 828282.
[43] J. Gu, L. Chen, R. Sun, J.-L. Wang, J. Wang, Y. Lin, S. Lei, Y. Zhang, D. Lv, F. Jiang, Y. Deng, J. P. Collman, L. Fu, *Front. Mol. Biosci.* **2022**, *9*, 815320.
[44] S. Paul, G. I. Lancaster, P. J. Meikle, *Prog. Lipid Res.* **2019**, *74*, 186.
[45] T. Fujino, M. S. Hossain, S. Mawatari, in *Peroxisome Biology: Experimental Models, Peroxisomal Disorders and Neurological Diseases*, (Ed: G. Lizard), Springer International Publishing, Cham, Berlin **2020**, pp. 195.
[46] Y. Otoki, S. Kato, K. Nakagawa, D. J. Harvey, L.-W. Jin, B. N. Dugger, A. Y. Taha, *Neuromolecular Med.* **2021**, *23*, 161.
[47] J. Lessig, B. Fuchs, *Curr. Med. Chem.* **2009**, *16*, 2021.
[48] A. M. Luoma, F. Kuo, O. Cakici, M. N. Crowther, A. R. Denninger, R. L. Avila, P. Brites, D. A. Kirschner, *Free Radical Biol. Med.* **2015**, *84*, 296.
[49] S. Sejimo, M. S. Hossain, K. Akashi, *Biochem. Biophys. Res. Commun.* **2018**, *503*, 837.
[50] M. Ifuku, T. Katafuchi, S. Mawatari, M. Noda, K. Miake, M. Sugiyama, T. Fujino, *J. Neuroinflammation* **2012**, *9*, 197.
[51] F. Dorninger, T. König, P. Scholze, M. L. Berger, G. Zeitler, C. Wiesinger, A. Gundacker, D. D. Pollak, S. Huck, W. W. Just, S. Forss-Petter, C. Pifl, J. Berger, *Hum. Mol. Genet.* **2019**, *28*, 2046.
[52] X. Q. Su, J. Wang, A. J. Sinclair, *Lipids Health Dis.* **2019**, *18*, 100.
[53] M. S. Hossain, S. Mawatari, T. Fujino, *Adv. Exp. Med. Biol.* **2020**, *1299*, 171.
[54] T. Fujino, T. Yamada, T. Asada, Y. Tsuboi, C. Wakana, S. Mawatari, S. Kono, *EBioMedicine* **2017**, *17*, 199.
[55] S. Mawatari, S. Ohara, Y. Taniwaki, Y. Tsuboi, T. Maruyama, T. Fujino, *Parkinson's Dis.* **2020**, *2020*, 2671070.
[56] T. Fujino, M. S. Hossain, S. Mawatari, *Adv. Exp. Med. Biol.* **2020**, *1299*, 195.
[57] T. T. Nguyen, T. T. Dung Nguyen, T. K. Vo, N.-M.-A. Tran, M. K. Nguyen, T. Van Vo, G. Van Vo, *Biomed. Pharmacother.* **2021**, *143*, 112117.

[58] K. Jagaran, M. Singh, *Int. J. Mol. Sci.* **2021**, *22*, 9082.
[59] T. B. Soares, L. Loureiro, A. Carvalho, M. E. C. D. R. Oliveira, A. Dias, B. Sarmento, M. Lúcio, *Prog. Neurobiol.* **2018**, *168*, 21.
[60] C. Martinelli, C. Pucci, M. Battaglini, A. Marino, G. Ciofani, *Adv. Healthcare Mater.* **2020**, *9*, 1901589.
[61] L. F. González, L. E. Bevilacqua, R. Naves, *Pharmaceutics* **2021**, *13*, 2055.
[62] H. Wu, J. Li, Q. Zhang, X. Yan, L. Guo, X. Gao, M. Qiu, X. Jiang, R. Lai, H. Chen, *Eur. J. Pharm. Biopharm.* **2012**, *80*, 368.
[63] H. Azhari, M. Younus, S. M. Hook, B. J. Boyd, S. B. Rizwan, *Int. J. Pharm.* **2021**, *600*, 120411.
[64] K. Ganapathy, I. Datta, S. Sowmithra, P. Joshi, R. Bhonde, *J. Cell. Biochem.* **2016**, *117*, 2719.
[65] Q. Wang, L. Zhang, X. Yuan, Y. Ou, X. Zhu, Z. Cheng, P. Zhang, X. Wu, Y. Meng, L. Zhang, *PLoS One* **2016**, *11*, e0163327.
[66] K. Lohner, P. Balgavy, A. Hermetter, F. Paltauf, P. Laggner, *Biochim. Biophys. Acta* **1991**, *1061*, 132.
[67] K. Lohner, A. Hermetter, F. Paltauf, *Chem. Phys. Lipids* **1984**, *34*, 163.
[68] H. Matsuki, E. Miyazaki, F. Sakano, N. Tamai, S. Kaneshina, *Biochim. Biophys. Acta* **2007**, *1768*, 479.
[69] A. West, V. Zoni, W. E. Teague Jr., A. N. Leonard, S. Vanni, K. Gawrisch, S. Tristram-Nagle, J. N. Sachs, J. B. Klauda, *J. Phys. Chem. B* **2020**, *124*, 828.